Electronic Materials

IMR KINKEN Research Highlights 2016

Antiferromagnetic Skyrmions

Topological spin textures such as skyrmions have been actively studied in ferromagnets over the past several years as they may become bits of information in future spintronic memory devices. We propose to study similar topological objects in antiferromagnets, in which the topology and the presence of two sublattices have a large effect on the dynamical and thermal properties.

Manipulating spin textures by electric and spin currents is one of the main challenges in the field of spintronics. Ferromagnetic skyrmions are attracting a lot of attention because they are small and not pinned as easily as domain walls when driven by electric currents. However, ferromagnetic skyrmions have disadvantages as well, such as the presence of stray fields and transverse motion, making it more difficult to employ them in spintronic devices. In this work, we propose a novel topological object, antiferromagnetic (AFM) skyrmion, and we explore its properties analytically and by micromagnetic simulations. This topological texture has no stray fields, as shown in Figs. 1(a) and (b), and it is more mobile than its ferromagnetic analogue.

We found that the Dzyaloshinskii–Moriya interaction, which comes from relativistic spin-orbit effects and generally favors spin spiral structures, stabilizes the AFM skyrmions. The AFM skyrmion radius dependes on the strength of the Dzyaloshinskii–Moriya interaction and temperature. Moreover, the thermal properties, such as the radius and diffusion constant, differ from those of ferromagnetic skyrmions. Because of the unusual topology, the AFM skyrmions do not experience a transverse (Magnus) force and therefore do not move transverse to an applied current [Fig. 1(c)], which makes them interesting candidates for spintronic applications [1]. These results can be understood in terms of a generalized Thiele equation, which describes soft modes of the skyrmion motion. This equation shows an exact cancelation of the Magnus force due to the presence of two AFM sublattices with opposite topological charges. It also leads to a larger diffusion constant of the AFM skyrmion as compared to its ferromagnetic counterpart.

The next step will be to investigate the efficiency of temperature gradients for the propagation of skyrmions in antiferromagnetic insulators and to develop a theory of spin-orbit torque driven AFM skyrmion motion in AFM/heavy metal bilayers.

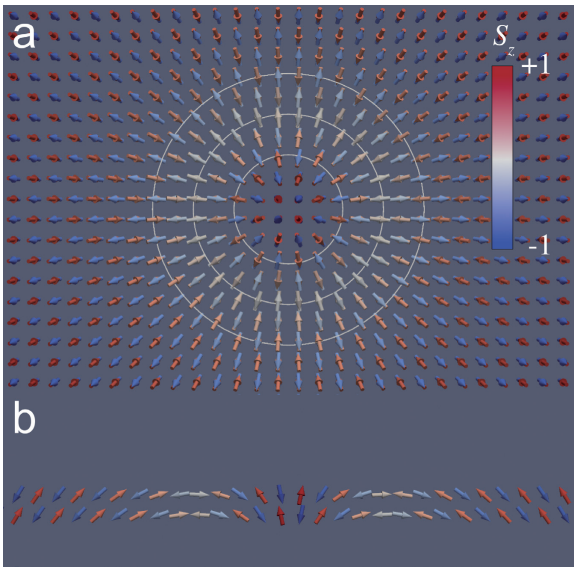

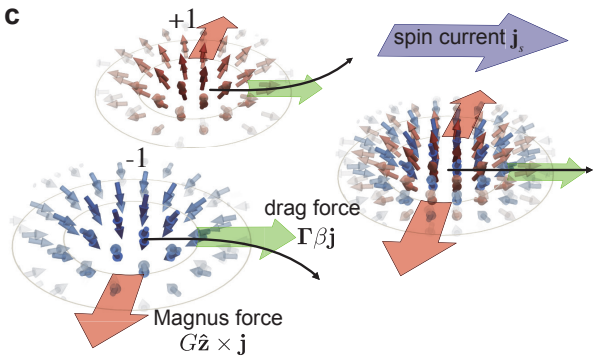

Fig. 1 (a)–(b) The spin texture of an antiferromagnetic (AFM) skyrmion: (a) top view of the AFM skyrmion and (b) skyrmion's cross section. (c) The AFM skyrmion is a composite topological object consisting of a skyrmion on one sublattice and an antiskyrmion on the other. This results in the cancelation of the overall Magnus force and therefore the absence of the topological Hall effect.

References

[1] J. Barker and O. A. Tretiakov, Phys. Rev. Lett. **116**, 147203 (2016)

Keywords: skyrmions, Dzyaloshinskii-Moriya interaction, antiferromagnets
Oleg Tretiakov (Theory of Solid State Physics Division)
E-mail: olegt@imr.tohoku.ac.jp
URL: http://www.bauer-lab.imr.tohoku.ac.jp/index_e.html

Fusion of Pulse Fields and Pulse X-ray Unveils New Charge Density Wave State

Development of a three-dimensional correlation of a charge density wave in $YBa_2Cu_3O_{6.67}$ was discovered by single-shot X-ray diffraction in high magnetic fields. The combination of the pulsed magnet and the intense pulse X-ray enabled us to pick up the extremely weak super-lattice modulation caused by the magnetic field-induced electronic phase transition.

High magnetic fields induce various electronic phase transitions such as metal–insulator, charge density wave (CDW), and valence-state transitions. Unique structural anomalies are associated with these transitions, but observations of such tiny changes of crystal symmetry and/or volume have been difficult. For example, CDW states appearing under high magnetic fields in Cu oxide superconductors have been intensively studied. However, direct observation of a CDW super-lattice peak has been made only in magnetic fields much lower than the upper critical fields. An ultimate tool to investigate such small lattice modulations in extremely high magnetic fields had been sought for long time.

In the current study, we combined two pulsed tools, a pulsed magnet and a pulsed X-ray source, to accomplish this difficult task. The magnetism division of IMR has developed an extremely compact split-pair magnet generating magnetic fields of over 30 T. The bore of the coil is only 3 mm and the length of the coil is as short as 25 mm. The SLAC National Accelerator Laboratory offers the most intense pulsed laser source on earth. When these two tools are combined, weak CDW peaks in $YBa_2Cu_3O_{6.67}$ can be detected clearly in a single-shot pulsed magnetic field [1]. It should be also noted that IMR offers a compact capacitor bank developed and assembled at the magnetism division. The “flying magnet” and the “rolling capacitor bank” make this fusion possible.

In the present experiments, a new CDW state with strong three-dimensional correlation was discovered. The index of this CDW state is given by (δ, 0, l), where δ is related to the localized charge modulation in the c-plane. Moreover, the index l was found to be an integer. This unique feature is in sharp contrast to the two-dimensional CDW peak found in lower magnetic fields at the (δ, 0, $l/2$) position, where the modulation pitch along the c-axis is doubled. The intensity of the l = integer peak increased rapidly in high magnetic fields, whereas that of the half-integer peak saturated in lower magnetic fields. The appearance of a state with localized electrons with such strong three-dimensionality shows the essential role of the strong electron correlation in the normal state of $YBa_2Cu_3O_{6.67}$ and the existence of a few competing interactions. The present experiment demonstrates the power of the new tool for investigating magnetic field-induced electronic transitions.

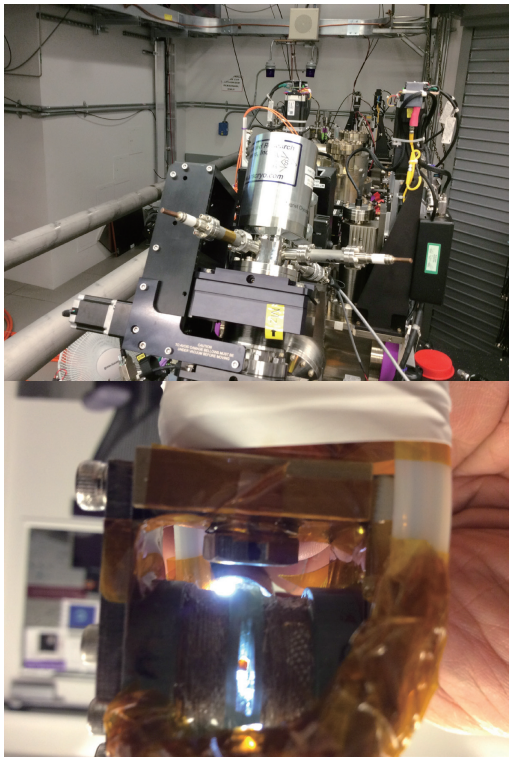

The figure shows the X-ray diffraction chamber used at Linac Coherent Light Source at SLAC National Accelerator Laboratory for a single-shot high-magnetic-field X-ray diffraction and the split-pair pulse coil mounted on the cold finger of the specimen.

References

[1] S. Gerber, H. Jang, H. Nojiri, S. Matsuzawa, H. Yasumura, D. A. Bonn, R. Liang, W. N. Hardy, Z. Islam, A. Mehta, S. Song, M. Sikorski, D. Stefanescu, Y. Feng, S. A. Kivelson, T. P. Devereaux, Z.-X. Shen, C.-C. Kao, W.-S. Lee, D. Zhu, and J.-S. Lee, Science **350**, 949 (2015).

Keywords: high magnetic field, superconducting, X-ray scattering
Hiroyuki Nojiri (Magnetism Division)
E-mail: nojiri@imr.tohoku.ac.jp
URL: http://www.hfpm.imr.tohoku.ac.jp/

Fluid-mechanical Spin-current Generation

Fundamental studies of spintronics focus on the manipulation and generation of spin currents. To generate spin currents, recent studies have utilized several interactions with electron spins in condensed matter; the key is angular momentum conversion. Here, we experimentally show that fluid-mechanical angular momentum enables us to generate spin currents.

Macroscopic mechanical rotation is the most common carrier of angular momentum. Mechanical rotation can interact with electron spins directly, as suggested by the Barnett effect, inducing spin polarization by mechanical rotation of a material object. However, generation of a spin current as a result of mechanical rotation has not been observed so far because it requires a mechanical rotation gradient, and producing such a rotation gradient is difficult in a solid. However, in fluid motion, and even in a conventional liquid flow in a pipe, we can easily generate mechanical rotation by using the vorticity, which is the local rotation of a liquid due to the viscosity near the inner wall [Fig. 1(a)]. Hence, as the liquid flows through the pipe, a spin current due to macroscopic motion is expected to be generated along the direction of the vorticity gradient, perpendicular to the pipe flow.

In the present study [1], to detect the spin current in a liquid, especially liquid metals (such as Hg and the gallium alloy $Ga_{62}In_{25}Sn_{13}$), we used the inverse spin Hall (ISH) effect, converting a spin current into electric voltage perpendicular to the spin-current direction through the spin-orbit interaction of electrons. Hence, in the pipe flow, the ISH voltage is expected to be generated along the flow direction [Fig. 1(a)]. Figure 1(b) shows the results of measurements of the voltage along the flow direction in the Hg pipe flow. A clear voltage signal appears when Hg is flowing. The sign of the signal is reversed upon reversing the flow direction; this unconventional voltage behavior is predicted for the ISH effect induced by the mechanical motion described above. We also examined the consistency of the current results with the theory on spin-current generation due to fluid motion [1].

This phenomenon is fundamentally new; it bridges the gap between spintronics and hydrodynamics, and it is expected to become a stepping-stone to expanding spintronic phenomena into fluids.

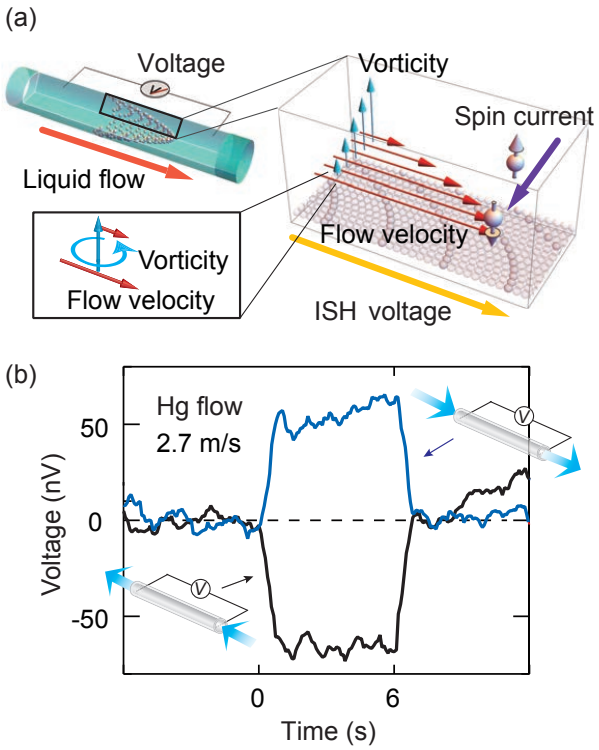

Fig. 1 (a) Concept of fluid-mechanical spin- current generation. Translational motion with different velocities in a local flow region exhibits local rotational motion whose angular velocity is proportional to the vorticity. The vorticity gradient becomes a spin-current source. (b) Time evolution of voltage signals induced by the Hg flow. The flow was started at 0 s and switched off at 6 s. The length and inner diameter of the pipe were 80 mm and 0.4 mm, respectively. The measurements were performed at room temperature.

References

[1] R. Takahashi, M. Matsuo, M. Ono, K. Harii, H. Chudo, S. Okayasu, J. Ieda, S. Takahashi, S. Maekawa, and E. Saitoh, Nature Phys. **12**, 52 (2016).

Keywords: spintronics, electronic material, spin current
Ryo Takahashi and Eiji Saitoh (Surface and Interface Research Division)
E-mail: takahashi.ryo@jaea.go.jp; eiji@imr.tohoku.ac.jp
URL: http://saitoh.imr.tohoku.ac.jp/

High-T_c Superconductivity of FeSe Emerges in Thinning Manner

Two-dimensional layered materials possess significant potential to exhibit intriguing physical properties by combining external electric fields. Iron selenide (FeSe) is a layered material that has received much attention because of its high superconducting transition temperature (high-T_c) when an atomic monolayer is deposited onto $SrTiO_3$. Here, we highlight a new approach to obtaining high-T_c superconductivity of ultrathin FeSe films by an electrochemical reaction in an electric double-layer transistor (EDLT). The EDLT allows layer-by-layer electrochemical etching of FeSe films down to an atomic monolayer and electrostatic control of the superconductivity.

FeSe is an iron-based superconductor with a superconducting transition temperature (T_c) of 8 K in bulk form [1]. Stacking of Se–Fe–Se atoms forms a layered crystal structure. The recent astonishing discovery of its high-T_c superconductivity with a large gap of approximately 20 meV corresponding to T_c = 65 K has sparked an explosion of investigations of atomic monolayers of FeSe deposited onto $SrTiO_3$ substrates by mainly *in-situ* characterization using photo-emission and scanning tunneling spectroscopies [2, 3]. However, the systematic thickness dependence of electrical measurements of the superconductivity and its electric field effect have not been addressed so far, mainly because of the experimental difficulty in obtaining *ex-situ* measurements for atomically thin films.

To overcome this issue, we applied the electric double-layer transistor (EDLT) technique with thick FeSe films grown by pulsed-laser deposition [4]. EDLTs were originally employed to investigate novel physical phenomena with significant charge carrier accumulation. Our team applied the EDLT technique to regulate the FeSe film thickness by an electrochemical reaction, enabling layer-by-layer etching down to an atomic monolayer. With decreasing thickness, a high-T_c superconductivity of 40 K surprisingly emerged in *ex-situ* electrical resistivity measurements (brown curve in Fig. 1). In addition, the systematic thickness dependence of the superconductivity was successfully revealed in our study. Moreover, electrical control of the superconductor-to-insulator transition was realized via control of the external electric field (from the red to the purple curves in Fig. 1). Our results point out the importance of electric-field-induced electronic band modulation for generating high-T_c superconductivity in FeSe.

This electrochemical etching approach could be applied to other layered materials. We believe this method is a powerful technique for exploring novel physical phenomena in two-dimensional layered systems.

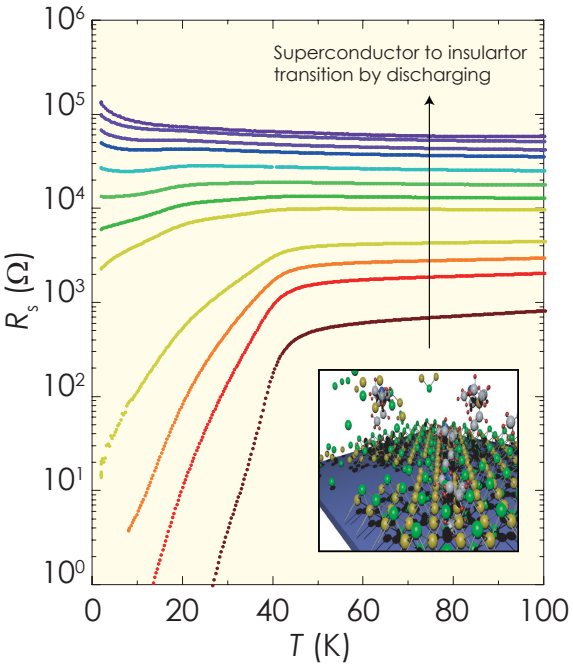

Fig. 1 Superconducting transition behavior in EDLT device upon applying an external electric field (brown curve). A decrease in the number of charge carriers (discharging) induced superconductor-to-insulator transition (from red to purple). (Inset) Schematic image of atomic layer of FeSe in ionic liquid.

References

[1] F. C. Hsu, J. Y. Luo, K. W. Yeh, T. K. Chen, T. W. Huang, P. M. Wu, Y. C. Lee, Y. L. Huang, Y. Y. Chu, D. C. Yan, and M. K. Wu, Proc. Natl. Acad. Sci. USA **105**, 14262 (2008).

[2] Q. Y. Wang, Z. Li, W. H. Zhang, Z. C. Zhang, J. S. Zhang, W. Li, H. Ding, Y. B. Ou, P. Deng, K. Chang, J. Wen, C. L. Song, K. He, J. F. Jia, S. H. Ji, Y. Y. Wang, L. L. Wang, X. Chen, X. C. Ma, and Q. K. Xue, Chin. Phys. Lett. **29**, 037402 (2012).

[3] S. He, J. He, W. Zhang, L. Zhao, D. Liu, X. Liu, D. Mou, Y. B. Ou, Q. Y. Wang, Z. Li, L. Wang, Y. Peng, Y. Liu, C. Chen, L. Yu, G. Liu, X. Dong, J. Zhang, C. Chen, Z. Xu, X. Chen, X. Ma, Q. Xue, and X. J. Zhou, Nature Mater. **12**, 605 (2013).

[4] J. Shiogai, Y. Ito, T. Mitsuhashi, T. Nojima, and A. Tsukazaki, Nature Phys. **12**, 42 (2016).

Keywords: superconducting, thin films, field-effect transistor
Junichi Shiogai (Low Temperature Physics Division)
E-mail: junichi.shiogai@imr.tohoku.ac.jp
URL: http://mu.imr.tohoku.ac.jp/index_en.html

Charge Degrees of Freedom under High Pressure in the Organic Dimer-Mott Insulator β′-(BEDT-TTF)$_2$ICl$_2$

Low-dimensional layered organic conductors are a promising class of materials that exhibit high-temperature superconductivity. Among them, an antiferromagnetic dimer-Mott insulator, β′-(BEDT-TTF)$_2$ICl$_2$, showed superconductivity at 14.2 K under 8 GPa. We performed optical conductivity measurements for β′-(BEDT-TTF)$_2$ICl$_2$ under high pressure, which revealed that charge fluctuations inside dimers play an important role in high-temperature superconductivity.

The organic conductor β′-(BEDT-TTF)$_2$ICl$_2$, which shows superconductivity at 14.2 K under high pressure (~8 GPa), has aroused significant interest because its transition temperature is the highest among organic superconductors known to date. At ambient pressure, β′-(BEDT-TTF)$_2$ICl$_2$ is a dimer-Mott (DM) insulator with an antiferromagnetic transition temperature, T_N, of 22 K. As typically seen in bandwidth-controlled Mott transition systems, β′-(BEDT-TTF)$_2$ICl$_2$ also exhibits superconductivity when the antiferromagnetic phase is suppressed by applying pressure. It is believed, therefore, that antiferromagnetic spin fluctuations play an essential role in high-T_c superconductivity.

To elucidate the effect of pressure on the superconductivity of β′-(BEDT-TTF)$_2$ICl$_2$, we measured the polarized infrared (IR) optical spectra under high pressure using a diamond anvil cell (DAC) [Fig. 1(a)] [1]. At ambient pressure, two characteristic bands due to intra- and interdimer charge transfers were observed in the IR spectra, indicating that this salt is a typical half-filled DM insulator at ambient pressure [Fig. 1(b)]. With increasing pressure, however, the intradimer charge transfer excitation shifted to much lower energies, indicating that the effective electronic state changes from half-filled to three-quarters-filled as a result of weakening of dimerization [Fig. 1(c)]. This implies that the system approaches a charge-ordered state under high pressure, in which charge degrees of freedom emerge as an important factor. The present results suggest that in addition to antiferromagnetic spin fluctuations, charge fluctuations inside dimers play an important role in high-temperature superconductivity.

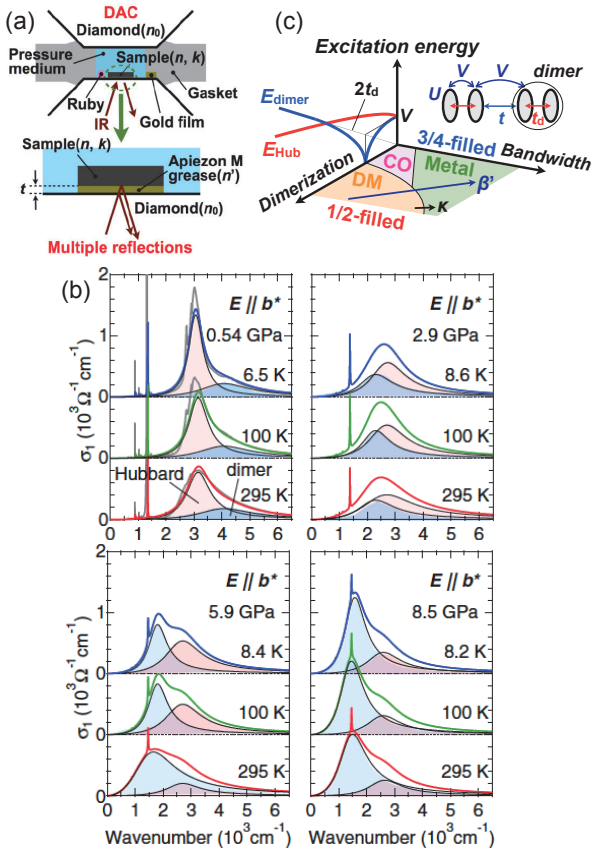

Fig. 1 (a) Experimental setup for the optical measurements under high pressure using a DAC. (b) Optical conductivity spectra of β′-(BEDT-TTF)$_2$ICl$_2$ measured in the DAC at various pressures. The gray lines in the upper left panel show the $\sigma_1(\omega)$ spectra measured at ambient pressure. (c) The schematic phase diagram expected in the extended Hubbard model with the molecular dimer degree of freedom is shown as functions of degree of dimerization and bandwidth. The excitation energies of the Hubbard and dimer bands are also shown as functions of degree of dimerization. In β′-(BEDT-TTF)$_2$ICl$_2$, when the pressure is applied, the system would follow the track drawn by the arrow.

References

[1] K. Hashimoto, R. Kobayashi, H. Okamura, H. Taniguchi, Y. Ikemoto, T. Moriwaki, S. Iguchi, M. Naka, S. Ishihara, and T. Sasaki, Phys. Rev. B **92**, 085149 (2015).

Keywords: organic, superconducting, optical properties
Kenichiro Hashimoto (Low Temperature Condensed State Physics Division)
E-mail: hashimoto@imr.tohoku.ac.jp
URL: http://cond-phys.imr.tohoku.ac.jp/index.html

Spin Fluctuations on a Triangular Lattice

In geometrically frustrated magnets, *spin liquid* states attract considerable interest. We quantitatively examined temporal magnetic correlations of the triangular lattice antiferromagnet $NiGa_2S_4$ through thirteen decades (10^{-13}–1 s) and elucidated that megahertz spin fluctuations last over an extended temperature regime.

Two-dimensional triangular lattices play a prominent role in the field of frustrated magnetism. Although it now seems clear that a conventional triangular lattice antiferromagnet has a long-range 120-deg order, irrespective of the spin quantum number, S, experiments on materials with generalized longer-range and spin-orbit interactions, as well as lattice distortions, point to a rich variety of phases in the vicinity of the ordered phase. In the quantum limit (S = 1/2) first considered by Anderson, experiments on organic materials suggested that a gapless spin liquid with a spinon Fermi surface may exist near the metal–insulator transition.

For larger spin quantum numbers, theoretical and experimental works have pointed to complex slow spin dynamics that are still poorly understood. Here, we focus on such dynamics in the S = 1 triangular lattice antiferromagnet $NiGa_2S_4$, which is distinguished by a two-dimensional incommensurate magnetic wave vector and the potential for spin-nematic interactions.

$NiGa_2S_4$ consists of neutral insulating layers held together by van der Waals forces [inset to Fig. 1(a)]. This curtails electron hopping between layers and leads to a strongly two-dimensional magnet. Within each layer, nickel ions with S = 1 reside on an equilateral triangular lattice. Upholding expectations of anomalous magnetism, the material does not exhibit conventional magnetic ordering down to a temperature T of 50 mK, and the in-plane correlation length gradually increases upon cooling but tends to remain at approximately 2.6 nm (7 lattice spacings) without a thermal anomaly [Fig. 1(a)].

In sharp contrast, *temporal* correlations feature clear thermal anomalies. Figure 1(b) shows the temperature dependence of the characteristic spin relaxation time in $NiGa_2S_4$. Using high-energy resolution inelastic neutron scattering, neutron spin echo, muon spin relaxation, and AC magnetometry, we provide evidence for emergent MHz spin dynamics over a wide range of temperatures [1]. We argue that such slow spin dynamics are associated with emergent topologically protected degrees of freedom inherent to incommensurate magnetism on the triangular lattice.

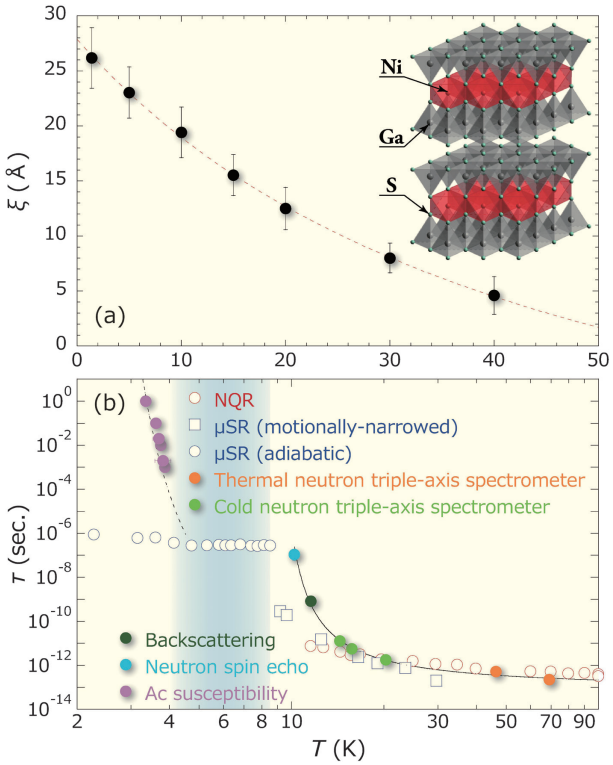

Fig. 1 Temperature dependence of (a) the spin correlation length and (b) characteristic spin relaxation time of $NiGa_2S_4$. The crystal structure of $NiGa_2S_4$ is depicted in the inset to (a). Above and below T^*= 8.5 K, the muon spin relaxation rates are in the motionally narrowed and adiabatic limits, respectively. Vogel–Fulcher behavior from the AC susceptibility measurements is given by the dotted curve. The dashed curve in (a) and the solid curve towards T^* in (b) are visual guides.

References

[1] Y. Nambu, J.S. Gardner, D.E. MacLaughlin, C. Stock, H. Endo, S. Jonas, T.J. Sato, S. Nakatsuji, and C. Broholm Phys. Rev. Lett. **115**, 127202 (2015).

Keywords: neutron scattering, triangular antiferromagnet, spin fluctuation
Yusuke Nambu (Metal Physics with Quantum Beam Spectroscopy Division)
E-mail: nambu@imr.tohoku.ac.jp
URL: http://qblab.imr.tohoku.ac.jp/

Dislocation-based Plasticity of Si

The classical idea that semiconductor silicon (Si) is brittle and cannot be deformed plastically at room temperature (RT) is now changing drastically. Recent experimental findings on the plasticity of Si from RT to its melting temperature (T_M) in terms of dislocation mobility and atomic core structure are reviewed.

Si is a key material in nano-sized devices for ultra-large-scale integrated (ULSI) circuits and for precision instruments for micro-electromechanical systems (MEMS). Knowledge of the elastic–plastic characteristics of Si is essential for controlling its crystallinity during various fabrication processes. Si is known to be typically ductile at temperatures higher than approximately $2/3T_M$, behavior that is governed by dislocation dynamics, whereas at lower temperatures, Si is brittle and susceptible to fracture without plastic deformation owing to the extremely low mobility of dislocations. Thus, there is a ductile-to-brittle transition (T_{BDT}) in the deformation mode at approximately 600–700°C.

Figure 1 shows the mechanical strength of Si crystals plotted against the reciprocal temperature from RT to 1300°C [1]. There are two regions with remarkable knees at approximately 400°C, showing a drastic change in the temperature dependence of the strength. At temperatures higher than the knees, Si deformed by compression or tension under atmospheric pressure, being ductile in conventional viewpoints. Surprisingly, Si deforms plastically even at temperatures from RT to the knee under specially arranged conditions. Small, thin plates (membranes) or micro-scale pillars whose thickness and diameter, respectively, are on the order of micrometers, can be deformed by compression or tension at atmospheric pressure. Bulk specimens can be compressively deformed without fracture under a confining (hydrostatic) pressure. Under these conditions, T_{BDT} decreases to temperatures close to RT. In low-temperature regions, the yield strength of Si is as high as 1.5 GPa, almost independent of the temperature, which is extremely different from its behavior at high temperatures. This feature leads to the so-called shuffle–glide controversy on the core structure of dislocations governing the plasticity of Si in the relevant temperature regions.

Plastic deformation of a crystal takes place through the generation, motion, and multiplication of dislocations in the crystal under stress. The processes are controlled by the dynamic properties of the dislocations. The dislocation velocity has been well determined experimentally as a function of stress and temperature.

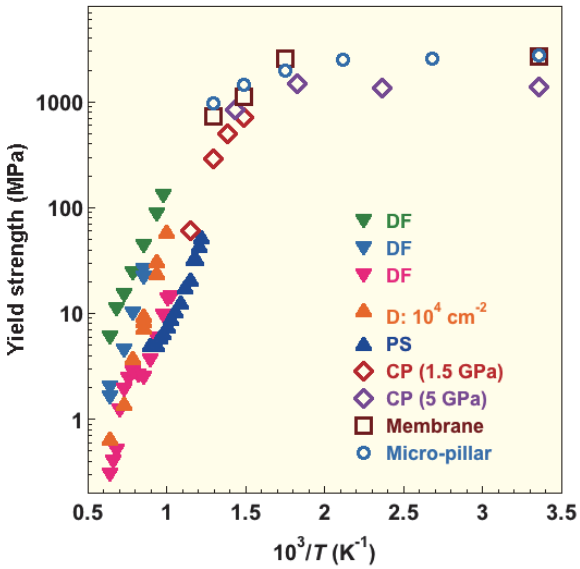

Fig. 1 Temperature dependence of strength of Si under various conditions [1]. DF: dislocation-free, D: dislocated, PS: pre-strained, CP: under confining pressure.

At high temperatures, the deformation processes are governed by the dynamic collective motion of glide-set dislocations. The process can be reproduced by the constitutive model with mutual interaction and self-multiplication of dislocations [2]. On the other hand, the generation of shuffle-set dislocations is favorable in deformation at the temperatures under the application of extremely high stress.

References

[1] I. Yonenaga, Eng. Fracture Mechanics **147**, 468 (2015).
[2] J. Cochard, I. Yonenaga, M. M'Hamdi, and Z. L. Zhang, J. Mech. Phys. Sol. **61**, 2402 (2014).

Keywords: defects, deformation, semiconducting
Ichiro Yonenaga (Physics of Crystal Defects Division)
E-mail: yonenaga@imr.tohoku.ac.jp
URL: http://lab-defects.imr.tohoku.ac.jp/

Measurement of Internal Electric Fields in Group-III Nitride Devices by Electroreflectance Spectroscopy

Nitride semiconductor-based devices have strong polarization-induced internal electric fields, which affect the device performance. To improve the device performance, it is important to design a device structure that takes the actual internal electric fields into consideration. In this study, the internal electric field was directly measured by electroreflectance spectroscopy.

Group-III nitride semiconductors exhibit a wurtzite crystal structure, and they have crystallographic polarity as a result of this crystal structure. The choice of crystallographic polarity is one of the key issues because it influences several properties in terms of the crystal growth and device characteristics. N-polar growth facilitates the growth of InGaN with a high InN-molar fraction. In a previous study, N-polar InGaN/GaN light-emitting diodes (LEDs) operating across the visible spectrum have been demonstrated [1].

Devices based on group-III nitride semiconductors often have polarization-induced electric fields, which affect device performance [2, 3]. In order to realize high-efficiency devices, the device structure has to be designed by taking into consideration the actual internal electric fields induced by the crystallographic polarization. Up to now, there has been no report on the direct measurement of such fields. In this study, electroreflectance (ER) spectroscopy was adopted to investigate the actual internal electric fields in III-polar and N-polar InGaN/GaN LEDs. A comparable study for LEDs fabricated on GaN with different crystal orientation is thus demonstrated for the first time.

In ER measurements, the phases of the ER spectra are affected with the direction of the internal electric fields. Schematic diagrams of the energy band profiles and dielectric constants for III-polar and N-polar InGaN/GaN quantum wells are shown in Fig. 1. In InGaN layers with different polarities, the directions of the built-in electric fields are opposite each other. Therefore, the phase of an ER signal will be different depending on the direction of the internal electric fields. Figure 2 shows the ER spectra for III-polar and N-polar LEDs. The phases of the ER signals from the InGaN layers were opposite each other in the III-polar and N-polar samples. By fitting the ER spectra, the internal electric fields were estimated to be +2.3 MV/cm and –1.1 MV/cm for N-polar and III-polar LEDs, respectively. In conclusion, ER spectroscopy is confirmed as an effective method to directly measure the actual internal electric fields.

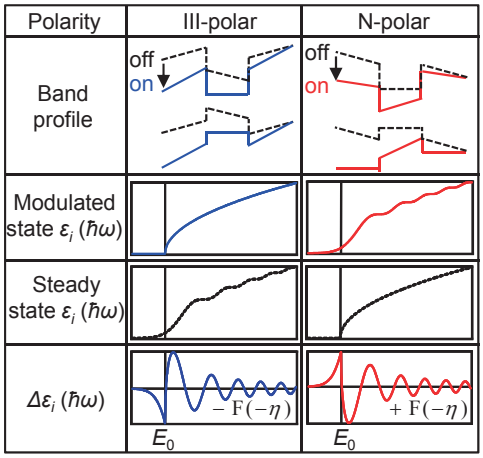

Fig. 1 Schematic diagrams of energy band profiles and difference between the steady-state and the modulated state in the imaginary part of dielectric constants ε_i ($\hbar\omega$).

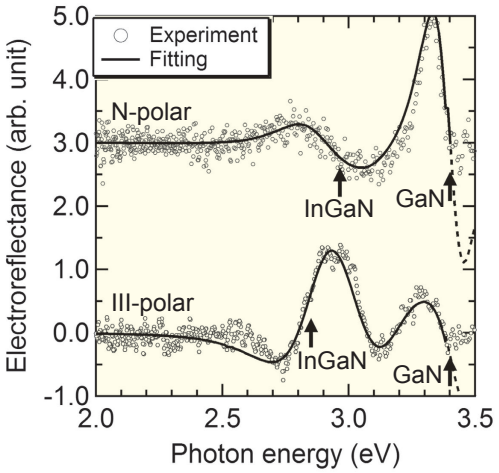

Fig. 2 ER spectra for III-polar and N-polar InGaN/GaN MQW-LEDs.

References

[1] K. Shojiki, T. Tanikawa, J. H. Choi, S. Kuboya, T. Hanada, R. Katayama, and T. Matsuoka, Appl. Phys. Express **8**, 061005 (2015).
[2] T. Aoki, T. Tanikawa, R. Katayama, T. Matsuoka, and K. Shiojima, Jpn. J. Appl, Phys. **5S**, 04EJ09 (2016).
[3] T. Tanikawa, K. Shojiki, R. Katayama, S. Kuboya, and T. Matsuoka, Jpn. J. Appl, Phys. **5S**, 05FJ03 (2016).

Keywords: crystal growth, optoelectronic, spectroscopy
Takashi Matsuoka (Physics of Electronic Materials Division)
E-mail: matsuoka@imr.tohoku.ac.jp
URL: http://www.matsuoka-lab.imr.tohoku.ac.jp/?TOPPAGE

Design of Rigid Molecular Magnetic Frameworks from a Combination of Chain and Layer

The design of three-dimensional (3D) magnetic pathways is a crucial point for the creation of molecular magnets. We have recently reported a new strategy for constructing 3D magnetic frameworks: π-type donor molecules, which could make a magnetic pathway, could be combined with π-type acceptor magnetic layers. This framework was named "π-stacked pillared layer frameworks" (π-stacked PLFs). In this framework, we can integrate a magnetic pathway, even in the inter-layer direction, through inserted paramagnetic molecules.

Layered magnetic frameworks, which are often producible in the synthesis of molecular magnets, are useful for designing hybrid materials with new functional molecules intercalated between layers; however, are disadvantage to creating high *T*c magnets. We previously reported a new class of molecular magnets made from a D2A formulation of paramagnetic electron-donor (D) units (paddlewheel-type diruthenium(II, II) unit; $[Ru_2^{II,II}]$) and electron-acceptor (A) units (tetracyano-*p*-quinodimethane derivatives; $TCNQR_x$) [1]. This type of compound mainly provided layered magnets, which made it difficult to control inter-layer interactions [2].

Here, we introduce a unique three-dimensional framework named a "π-stacked pillared layer framework (π-stacked PLF)" for magnet design. Two types of low-dimensional magnet frameworks, a D2A magnetic layer noted above and a charge transfer $[FeCp^*_2]^+TCNQ^{\bullet-}$ columnar magnet ($[FeCp^*_2]^+$ = decamethylferrocenium), were integrated in order to fabricate the magnet [3]. $[FeCp^*_2]^+TCNQ^{\bullet-}$ was reported by Miller et al. and is known to form a π-stacking alternating column comprising ferromagnetically coupled Coulombic sets $[FeCp^*_2]^+$ and $TCNQ^{\bullet-}$ with $S = ½$ [4]. When combined with the layered D2A, the $[FeCp^*_2]^+$ unit acts as a π-stacking pillar for the D2A layers sandwiched between $TCNQ^{\bullet-}$ moieties, resulting in a π-stacking PLF with the formula $[FeCp^*_2][\{Ru_2\}_2TCNQ]$ (Fig. 1).

The π-stacked PLF compound exhibited a ferrimagnetic phase transition at 82 K (Fig. 1), which could be increased to 107 K by applying a pressure of 12.5 kbar. These results imply that the inserted spin of $[FeCp^*_2]^+$ affected the formation of the three-dimensional spin arrangement. This synthetic strategy employing a combination of layers and chains is widely useful for magnet design based on molecular assemblies.

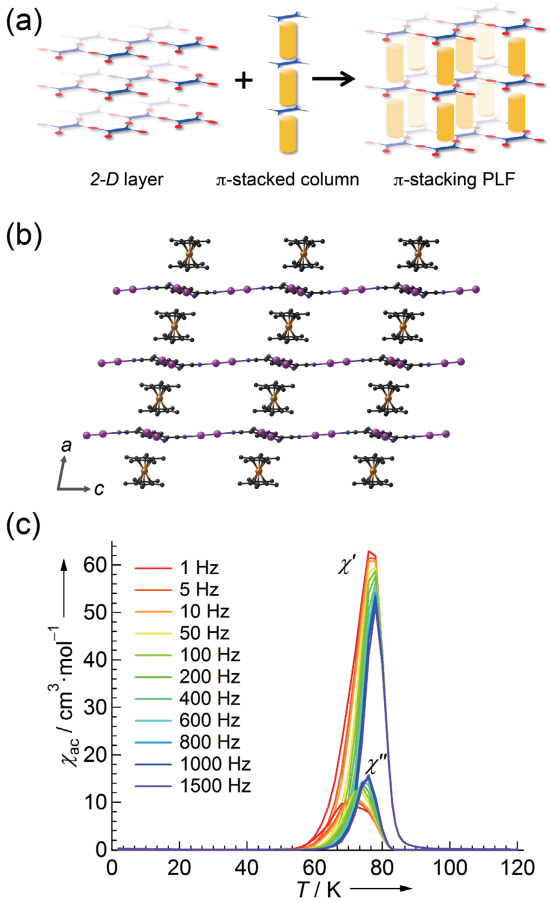

Fig. 1 (a) Schematic representation of the design strategy for π-stacked PLF. (b) The layered structure of the obtained π-stacked PLF compound. (c) Temperature-dependence of ac susceptibilities (in-phase χ′ and out-of-phase χ″) of the compound.

References

[1] H. Miyasaka, Acc. Chem. Res. **46**, 248 (2013).
[2] H. Miyasaka, T. Izawa, N. Takahashi, M. Yamashita, and K. R. Dunbar, J. Am. Chem. Soc. **128**, 11358 (2006).
[3] H. Fukunaga and H. Miyasaka, Angew. Chem. Int. Ed. **54**, 569 (2015).
[4] G. A. Candela, L. J. Swartzendruber, J. S. Miller, and M. J. Rice, J. Am. Chem. Soc. **101**, 2755 (1979).

Keywords: magnetic properties, crystal structure, ferromagnetic
Hitoshi Miyasaka (Solid-State Metal-Complex Chemistry Division)
E-mail: miyasaka@imr.tohoku.ac.jp
URL: http://www.miyasaka-lab.imr.tohoku.ac.jp/

Enhanced Output of the Giant Magnetoresistance Junction for Hard Disc Drive Applications

Current perpendicular to plane giant magnetoresistance (CPP-GMR) junctions are a key element for future reading head applications of hard disk drives with an areal recording density of several tera-bit per square inches, which is being demanded for storing the enormous amount of data present in society. We succeeded in enhancing the device output of the CPP-GMR junctions using half-metallic Heusler alloy electrodes and a newly developed Ag-Mg alloy spacer material.

In the last decade, there has been a drastic increase in the amount of information handled by society. Hard disc drives (HDDs) are one of the major storage devices with high data retention and low cost. It is necessary to develop HDDs of several tera-bit per square inches areal density for supporting this information. Toward this aim, it is necessary to enhance the sensitivity of the reading head devices. The current perpendicular-to-plane giant magnetoresistance (CPP-GMR) junction is expected to have useful applications in future HDDs [1]. It has been demonstrated that CPP-GMR junctions using half-metallic cobalt (Co)-based Heusler alloys and a silver (Ag) spacer layer exhibit a large device output compared with conventional 3*d*-transition-metal-based junctions [2, 3]. In this work, we have developed a new non-magnetic spacer layer, Ag-Mg alloy, which provides a larger device output than the previously used Ag spacer layer [4].

Figure 1 (a) shows a high-angle annular dark field scanning transmission electron microscope (HAADF-STEM) image of a layered film for the CPP-GMR junction, in which a Ag-Mg spacer layer is sandwiched with Co_2(Fe-Mn)Si Heusler alloy electrodes. Epitaxial growth and well-defined interfaces are clearly confirmed by the image. A HAADF-STEM image of a junction used for measuring the CPP-GMR effect is shown in Fig. 1 (b), and it is confirmed that a sub-micrometer-scaled junction was successfully fabricated. A typical result of the CPP-GMR effect is shown in Fig. 2 (a): The resistance of the junction clearly changed depending on the configuration of the magnetizations for the Co_2(Fe-Mn)Si electrodes, which is schematically described above the graph. The performance of the junction was characterized by investigating the bias voltage dependence of the output voltage (Fig. 2 (b)). The output of the newly developed Ag-Mg-spacer junction is about 25% larger than that of the conventional Ag-spacer. Our material can contribute to the development of next generation HDD-reading heads.

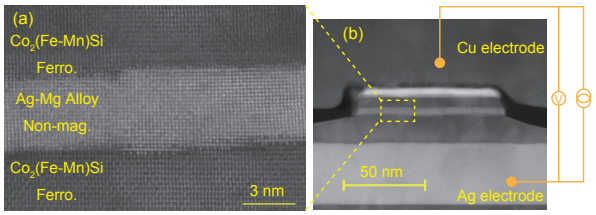

Fig. 1 (a) High-angle annular dark field scanning transmission electron microscope (HAADF-STEM) images of a Co_2(Fe-Mn)Si/Ag-Mg/Co_2(Fe-Mn)Si layered film, and (b) a CPP-GMR junction. Copyright (2015) The Japan Society of Applied Physics.

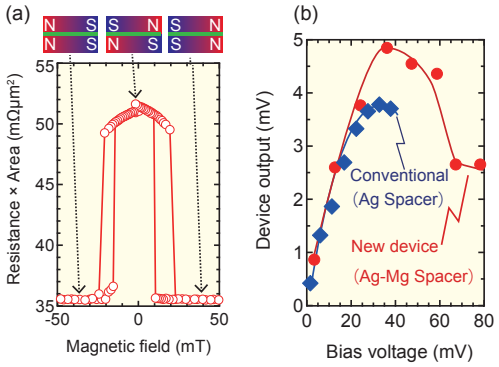

Fig. 2 (a) A CPP-GMR curve of a junction. High resistance state is observed for the anti-parallel magnetization configuration. (b) Device outputs as a function of the applied bias voltage for Ag spacer (diamond) and Ag-Mg spacer (circle) junctions. Copyright (2015) The Japan Society of Applied Physics.

References

[1] M. Takagishi, K. Yamada, H. Iwasaki, H. N. Fuke, and S. Hashimoto, IEEE Trans. Magn. **46**, 2086 (2010).

[2] Y. Sakuraba, M. Ueda, Y. Miura, K. Sato, S. Bosu, K. Saito, M. Shirai, T. J. Konno, and K. Takanashi, Appl. Phys. Lett. **101**, 252408 (2012).

[3] S. Li, Y. K. Takahashi, T. Furubayashi, and K. Hono, Appl. Phys. Lett. **103**, 042405 (2013).

[4] H. Narisawa, T. Kubota, and K. Takanashi, Appl. Phys. Express **8**, 063008 (2015).

Keywords: magnetoresistance, half-metal, spintronics
Koki Takanashi (Magnetic Materials Division)
E-mail: koki@imr.tohoku.ac.jp
URL: http://magmatelab.imr.tohoku.ac.jp/

Which Crystal Site Do Impurities Adore?

Crystal sites for impurities in lithium niobates (LN) were revealed by combining lattice constant measurements with thermodynamic constraints. Divalent and trivalent impurities were located at Li sites in LN, whereas tetravalent impurities were located at Nb sites. This result provides good clues for suppressing point defects, which enhances optical application of LN.

Lithium niobate ($LiNbO_3$: LN) is a ferroelectric material that shows excellent and versatile properties. LN has therefore been used as a substrate for nonlinear optical devices, as well as for surface acoustic wave devices. LN crystals are normally grown from the congruent melt to obtain a homogeneous composition. Because congruent LN (c-LN) contains more Nb than stoichiometric LN, excess Nb generates intrinsic point defects at Li sites. In the "Li site vacancy model" (Fig. 1) [1], intrinsic defects are antisite Nb (Nb_{Li}) and vacancies (V_{Li}) at Li sites. In particular, Nb_{Li} causes photorefractive damage, which hinders optical application of LN. Regarding this problem, doping impurities such as MgO were found to be effective for increasing the damage threshold [1]. However, it is not fully understood into which site impurities are incorporated and how impurities decrease the Nb_{Li} concentration. Here, the selection of impurity sites and Nb_{Li} behavior in impurity-doped c-LN were investigated by analyzing the defect structures, i.e., configurations of point defects, including impurities and intrinsic defects. The defect structures were determined by lattice constant measurements [2] combined with thermodynamic constraints [3].

Several defect structures of impurity-doped LN are possible depending on the occupancy of the impurities and the intrinsic defects in crystal sites. Among them, unfeasible defect structures can be excluded by considering thermodynamic constraints, that is, by evaluating the degrees of freedom in each crystal site [3]. The degrees of freedom are obtained by subtracting the number of thermodynamic constraints from the number of parameters. The number of parameters at each site corresponds to the number of elements, including defects such as antisite defects and vacancies. Meanwhile, thermodynamic constraints include mass conservation at each site and the element exchange in equilibrium [3]. The thermodynamic analysis revealed that only structures A and B (Fig. 1) are feasible out of the six models.

In structure A, impurities locate at the Li site where V_{Li} and Nb_{Li} also exist. In structure B, Impurities locate at the Nb site while V_{Li} and Nb_{Li} exist at the Li site.

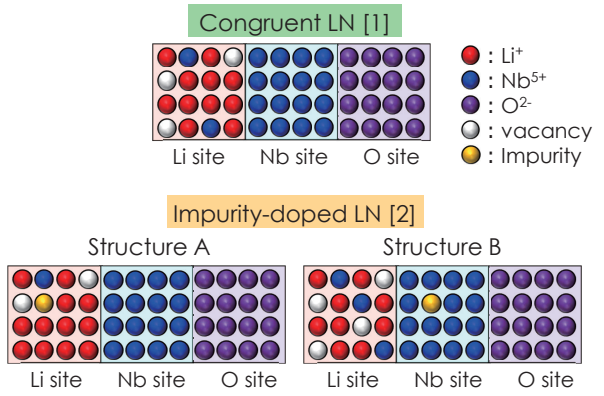

Fig. 1 Defect structures of congruent LN and impurity-doped LN.

Because the relationship between impurity concentration and lattice constants for structures A and B differ, the defect structures can be differentiated by analyzing lattice constant variations with impurity concentration. The results show that the defect structure of divalent and trivalent impurities, (Mg^{2+}, Zn^{2+}, Co^{2+}, Fe^{3+})-doped c-LN, employs structure A, whereas tetravalent impurities, (Zr^{4+}, Ti^{4+}, Ce^{4+})-doped c-LN, has structure B. The Nb_{Li} concentration increases with increasing tetravalent impurity concentration. In contrast, the Nb_{Li} concentration decreases with increasing divalent and trivalent impurities. It is the valence of an impurity that determines the location of impurities, whether they will be attracted to the Li site or the Nb site.

References

[1] T. Volk and M. Wöhlecke, "*Lithium Niobate Defects, Photorefraction and Ferroelectric Switching*" (Springer, 2008).

[2] C. Koyama, J. Nozawa, K. Maeda, K. Fujiwara, and S. Uda, J. Appl. Phys. **117**, 014102 (2015).

[3] S. Uda, "Chapter 4; Stoichiometry of oxide crystals", *Handbook of Crystal Growth, Vol. IA: Fundamentals 2nd Ed.* (Elsevier, 2014), Edited by T. Nishinaga.

Keywords: oxide, doping, defects
Chihiro Koyama and Satoshi Uda (Crystal Chemistry Division)
E-mail: uda@imr.tohoku.ac.jp
URL: http://www.uda-lab.imr.tohoku.ac.jp/index.html

Heaviest Electron Detected by Quantum Oscillations

In heavy fermion physics, Yb compounds attract much interest because they are hole analogues to Ce compounds. Here, the heaviest electrons in $YbCu_2Si_2$ were detected by quantum oscillation measurements. It was found that valence fluctuations play a key role in the heavy electronic state, although $YbCu_2Si_2$ at ambient pressure is far from the magnetic quantum critical point.

The de Haas–van Alphen (dHvA) effect, which is the quantum oscillation in magnetization, is one of the most powerful experimental probes for detecting Fermi surfaces. The frequency is proportional to the cross-sectional area of the Fermi surface, and thus one can precisely determine the topology of the Fermi surface by rotating the field angle. Effective masses can also be obtained for each Fermi surface, meaning that the heavy electronic state can be directly observed microscopically.

dHvA experiments have been extensively done for Ce compounds, and the heavy electronic states have been established. The phenomena are basically understood in terms of the competition between the Kondo effect and the Ruderman–Kittel–Kasuya–Yosida (RKKY) interaction. The magnetic quantum critical point and the novel quantum phase, including the superconductivity, are the central issues in correlated electron systems. However, in Yb compounds, which are hole analogues to Ce compounds, Fermi surfaces with heavy electronic states are not very well understood experimentally because the dHvA experiments require a high-quality sample, a high field, and low temperatures.

In this study, we focused on the intermediate-valence-fluctuating compound $YbCu_2Si_2$, which has no magnetic order at ambient pressure. The electronic specific heat coefficient is 150 mJ/K^2 mol, indicating a heavy electronic state. However, the band calculation, which does not include the many-body effect, resulted in a value of only 15 mJ/K^2 mol. Thus, a heavy Fermi surface with a 10-times-larger effective mass was expected in the experiments.

We performed the dHvA experiments using a high-quality single crystal of $YbCu_2Si_2$ under extreme conditions at temperatures down to 30 mK and at high fields up to 15 T [1]. Figure 1 shows the dHvA oscillation and its fast Fourier transform (FFT) spectrum. The dHvA branches denoted as α, β, γ, and ε correspond to the main Fermi surfaces. Among them, branch β is the heavy Fermi surface, with 43 m_0 (m_0: rest mass of electron), which

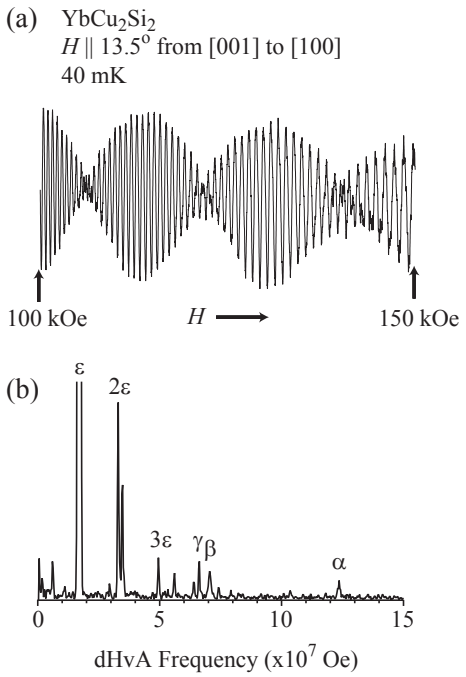

Fig. 1 Typical dHvA oscillation and its FFT spectrum in $YbCu_2Si_2$. Branch β has the heaviest cyclotron effective mass.

corresponds to the cylindrical Fermi surface centered at the X point in the Brillouin zone for a body-centered tetragonal structure. To our knowledge, the effective mass of 43 m_0 is the heaviest mass detected experimentally in dHvA studies of Yb compounds. Interestingly, the heavy mass in $YbCu_2Si_2$ is insensitive to the magnetic field. This is probably owing to the fact that $YbCu_2Si_2$ is a valence-fluctuating compound at ambient pressure, which is far from the magnetic quantum critical point ($P_c \approx 8$ GPa).

This work was done in collaboration with F. Honda, Y. Homma, D. X. Li, R. Settai, H. Harima, and Y. Onuki.

References

[1] D. Aoki, F. Honda, Y. Homma, D. X. Li, R. Settai, H. Harima, and Y. Onuki, J. Phys. Soc. Jpn. **84**, 035002 (2015).

Keywords: Fermi surface, heavy fermion
Dai Aoki (Actinide Materials Science Division)
E-mail: aoki@imr.tohoku.ac.jp
URL: http://actinide.imr.tohoku.ac.jp/

Effect of Ti Concentration on Chemically Ordered Regions in $Pb(Mg_{1/3}Nb_{2/3})O_3$–$PbTiO_3$ Epitaxial Thin Films

Although controversies still exist, the relaxor phenomenon in $Pb(Mg_{1/3}Nb_{2/3})O_3$ (PMN) is believed to arise from a heterogeneous structure consisting of a polar nano-region (PNR) and a chemically ordered region (COR). In the PNR, Mg and Nb are randomly arranged, thus giving rise to frustration, which is the origin of the phenomenon. In the CNR, these elements are ordered, and thus they inhibit the fluctuation. In this study, we investigated the effects of Ti substitution on the stability of CORs.

We prepared $(1 - x)Pb(Mg_{1/3}Nb_{2/3})O_3$–$xPbTiO_3$ (PMN–xPT) thin films by a chemical solution deposition process on $SrTiO_3$ (001) single-crystal substrates [1, 2]. The morphotropic phase boundary (MPB) was located at approximately x = 0.6. Our X-ray diffraction studies revealed that the deposited films were pseudocubic up to approximately x = 0.5, whereas tetragonality increased beyond this composition, suggesting a phase transformation [3]. This means that COR regions may exist below this value, and accordingly, we carried out structural examinations by using transmission electron microscopy (TEM).

The electron diffraction (ED) patterns from PMN–xPT specimens with x = 0–0.5 exhibited superlattice reflections at 1/2 1/2 1/2 and other corresponding positions, indicating the formation of CORs. It was also noted that the intensities of the superlattice reflections decreased with increasing Ti content, x. However, the ED patterns only gave an average structure; real-space examination was needed.

Figures 1 (a), (b), and (c) show high-angle annular detector dark-field (HAADF) scanning transmission electron microscope (STEM) images of PMN–xPT films with x = 0, 0.4, and 0.5, respectively. (Each set consists of wide-view images, magnified images, and diffractograms.) Because an HAADF-STEM image is basically that of Z-contrast, chemical ordering can be directly estimated by the intensity variations of the atomic images. The CORs thus obtained are indicated by solid rectangles in Fig. 1. As seen in the figure, each COR extends only up to 2 nm, or several unit cells, and they are distributed randomly within the film. It is also evident that an increase in Ti content led to the suppression of CORs. The driving force for the growth of CORs has its origin in the strain resulting from the difference of B-site cation radius, Mg^{2+}:0.072 nm and Nb^{5+}:0.067 nm, as well as in the electrical neutrality (Mg^{2+}:Nb^{5+} = 1:2). Overall, it can be said that CORs have intrinsic structural frustration and that Ti^{4+} mediates this situation.

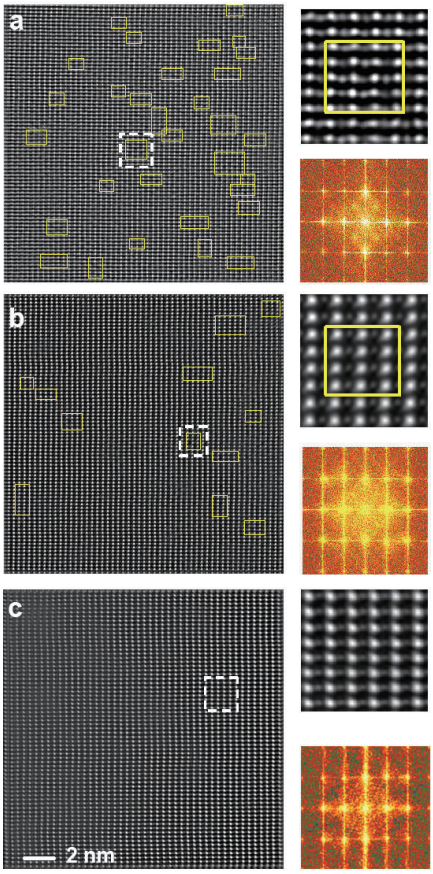

Fig. 1 Atomic-resolution HAADF-STEM images of (a) PMN, (b) PMN–0.4PT, (c) PMN–0.5PT. Diffractograms of the images and magnified images of a typical region marked with the white broken squares are also displayed. The solid lines in the HAADF-STEM images show CORs.

References

[1] T. Kiguchi, Y. Misaka, M. Nishijima, N. Sakamoto, N. Wakiya, H. Suzuki, and T. J. Konno, J. Ceram. Soc. Jpn. **121**, 236 (2013).
[2] Y. Misaka, T. Kiguchi, K. Sato, T. Nishimatsu, T. Yamada, N. Usami, and T. J. Konno, Key Eng. Mater. **582**, 19 (2014).
[3] C. Fan, T. Kiguchi, A. Akama, and T. J. Konno, J. Ceram. Soc. Jpn. **123**, 565 (2015).

Keywords: dielectric properties, nanostructure, transmission electron microscopy (TEM)
Takanori Kiguchi (Materials Science of Non-Stoichiometric Compounds Division)
E-mail: tkiguchi@imr.tohoku.ac.jp
URL: http://konno-lab.imr.tohoku.ac.jp/index.html